








Using large language models for parametric shape optimization

Xinxin Zhang ¹, Zhuoqun Xu ¹, Guangpu Zhu ¹, Chien Ming Jonathan Tay ¹, Yongdong Cui ¹, Boo Cheong Khoo ¹ and Lailai Zhu ^{1,*}

¹*Department of Mechanical Engineering, National University of Singapore, 117575, Singapore*
(Dated: December 12, 2024)

Recent advanced large language models (LLMs) have showcased their emergent capability of in-context learning, facilitating intelligent decision-making through natural language prompts without retraining. This new machine learning paradigm has shown promise in various fields, including general control and optimization problems. Inspired by these advancements, we explore the potential of LLMs for a specific and essential engineering task: parametric shape optimization (PSO). We develop an optimization framework, LLM-PSO, that leverages an LLM to determine the optimal shape of parameterized engineering designs in the spirit of evolutionary strategies. Utilizing the “Claude 3.5 Sonnet” LLM, we evaluate LLM-PSO on two benchmark flow optimization problems, specifically aiming to identify drag-minimizing profiles for 1) a two-dimensional airfoil in laminar flow, and 2) a three-dimensional axisymmetric body in Stokes flow. In both cases, LLM-PSO successfully identifies optimal shapes in agreement with benchmark solutions. Besides, it generally converges faster than other classical optimization algorithms. Our preliminary exploration may inspire further investigations into harnessing LLMs for shape optimization and engineering design more broadly.

I. INTRODUCTION

Shape optimization is a field of mathematical and computational design aimed at determining the best geometric configuration of a domain to optimize a given objective while satisfying constraints. It finds applications across engineering and science, from aerodynamic design [1] to structural analysis [2, 3], where efficient and innovative shapes are crucial for performance enhancement. By leveraging tools such as numerical simulations, optimization algorithms, and sensitivity analysis, shape optimization provides a systematic approach to addressing complex real-world design problem [4, 5].

A central branch of this field is parametric shape optimization (PSO), which represents the shape of a target design using a finite set of predefined parameters [6]. This method streamlines shape representations by condensing them into a manageable number of variables, thereby facilitating efficient optimization through various algorithms. Typically, these optimization algorithms are categorized into two groups: gradient-based and non-gradient-based [7].

Gradient-based methods involve computing the first-order or higher-order derivatives of performance metrics relative to shape parameters. These derivatives are utilized to guide the search direction towards an improved geometric configuration. Notable applications include using the steepest descent algorithm for optimizing hydraulic axisymmetric bodies in laminar flows [8], sequential linear programming for reducing stress concentrations in shoulder fillets [9], quasi-Newton methods for aerodynamic wing design [10], and sequential quadratic programming for shape optimization in various contexts

such as solid shell structures [11], cooling films [12], and solar reactors [13].

Alternatively, non-gradient-based heuristic algorithms also have shown significant potential for optimization [14]. They typically employ populations of candidate solutions to globally explore the solution space, iteratively evolving them through nature-inspired processes. As arguably the most common heuristic method, genetics algorithm (GA) mimics the evolutionary process of species and has proven effective in various shape optimization tasks. Applications of GAs span from optimizing the structural integrity of spanners and flanges for enhanced stress distribution [15], to improving the acoustic performance of sound absorbers [16], and advancing the design of robotic arms for increased maneuverability [17]. Other notable heuristic methods include simulated annealing [18], ant colony optimization [19], bat algorithm [20], sequential harmony search [21], and imperialist competitive algorithm [22], among many others.

With the advent and subsequent popularity of machine learning (ML) algorithms, their applications in shape optimization have garnered significant attention [23]. Among ML paradigms, supervised learning, trained on labeled datasets, has been extensively utilized to develop surrogate models that accelerate shape optimization at substantially reduced costs. Examples include minimizing wind effects on civil structures [24], reducing hydraulic drag on symmetric bodies [8], and enhancing the energy efficiency of bidirectional impulse turbines [25]. Leveraging inherent data structures without requiring explicit labels, unsupervised learning facilitates the reduced-order modeling of shape-induced physical fields [26, 27] or the shape itself [28], thereby enhancing optimization efficiency. Additionally, reinforcement learning (RL), a popular ML paradigm known for applications in robotic control [29] and gaming [30], has also been applied to shape optimization. For instance, [31] reports on optimizing missile control surfaces using RL,

* lailai_zhu@nus.edu.sg

and subsequent research has extended RL applications to airfoil design [32, 33], wind-sensitive building optimization [31], and heat exchanger optimization [34].

In-context learning (ICL) has recently emerged as a new ML paradigm, arising as an emergent capability of large language models (LLMs) when both the scale of their training datasets and model architectures surpass certain thresholds [35]. Unlike traditional paradigms, ICL allows LLMs to perform tasks based solely on provided contextual information, without the need for explicit retraining [36]. Consequently, LLMs have already shown great potential in various domains such as robotics [37, 38], industrial control [39], and general-purpose optimization [40–42]. Inspired by the success of LLMs as decision-makers in these applications, we are motivated to explore their potential in PSO—a methodology we propose and investigate in this work, referred to as LLM-PSO. Specifically, our study focuses on two PSO problems involving fluid motion and dynamics, although the approach itself is readily applicable to other fields beyond fluid dynamics.

II. RELATED WORKS

A. LLM for mechanics

LLMs open up new possibilities for addressing domain-specific challenges, including those in fluid mechanics and mechanics more broadly. For instance, [43] introduced MechGPT, a foundational model for mechanical and material science that can articulate related knowledge using natural language inputs. Similarly, [44] proposed a ChatGPT-assisted framework that enables the use of natural language descriptions to guide research tasks exemplified by airfoil shape optimization and physics-informed neural network training. Furthermore, Kim et al. [45] prompted ChatGPT-4 to generate MATLAB code for solving a two-dimensional seepage flow problem using a finite-difference method. Extending the scope further, MetaOpenFOAM [46] leveraged multi-agent LLM collaboration to streamline computational fluid dynamics tasks, covering mesh preprocessing, simulation, and post-processing.

In addition to serving as assistants to existing tools, LLMs can be directly utilized for scientific exploration, such as performing symbolic regression to derive the Navier-Stokes equations [47] and predicting flow fields by leveraging their temporal autoregressive capabilities [48]. Collectively, these research efforts highlight the burgeoning applicability of LLMs in fluid mechanics and general mechanical applications.

B. LLM for general optimization

LLMs excel at decision-making by interpreting textual input, thereby supporting the solution of general opti-

mization problems. For example, Guo et al. [40] directly prompted LLMs to mimic classic optimization algorithms such as gradient descent and hill climbing for the minimizing the values of least squares functions. Similarly, Google DeepMind [41] iteratively prompted LLMs to generate new solutions based on previous solutions and evaluations at each optimization step, achieving optimal parameter estimation for linear regression and determining the shortest path in the traveling salesman problem. Similar applications include LLM-based hyperparameter tuning [42] and supply chain optimization [49]. Furthermore, Liu et al. [50] combined LLMs with GAs, employing LLMs as the evolutionary operator, which demonstrated better performance compared to [41] in traveling salesman problems. Various approaches to leveraging LLMs to enhance classical optimization algorithms, such as evolutionary strategies [51, 52], Bayesian optimization [53], and guided local search [54], have also been explored. Moreover, LLMs have been employed to generate and design new optimization algorithms [55–58]. However, these applications primarily address general mathematical optimization problems and have not yet explored the potential of LLMs for shape optimization or broader engineering design.

C. Generative AI for engineering design

As a broader category encompassing LLMs, generative artificial intelligence (AI) has already harnesses its powerful generative capacity for optimizing engineering design [59]. By acting as a robust shape generator, generative AI has demonstrated its potential to improve design efficiency and foster innovation. Common generative AI models used in engineering design include generative adversarial networks (GANs) and diffusion models [60]. For instance, GANs have been applied to aerodynamic optimization [1, 61, 62] and building layout design [63]. More recently, diffusion models, notably Shap-E [64], have supported applications like automated vehicle design via natural language description [65, 66]. Similar research includes diffusion-based models for the mechanical structures optimization [67], building interior design [68], and airfoil shape optimization [69].

D. Attempting LLMs for shape optimization

In summary, LLMs serve as decision-makers for addressing general-purpose optimization problems. Concurrently, their siblings—GANs and diffusion models—have been adopted in engineering design, invoking us to contempt whether LLMs possess similar potential. Hence, we attempt here exploring LLMs’ decision-making abilities for a specific design task—parametric shape optimization.

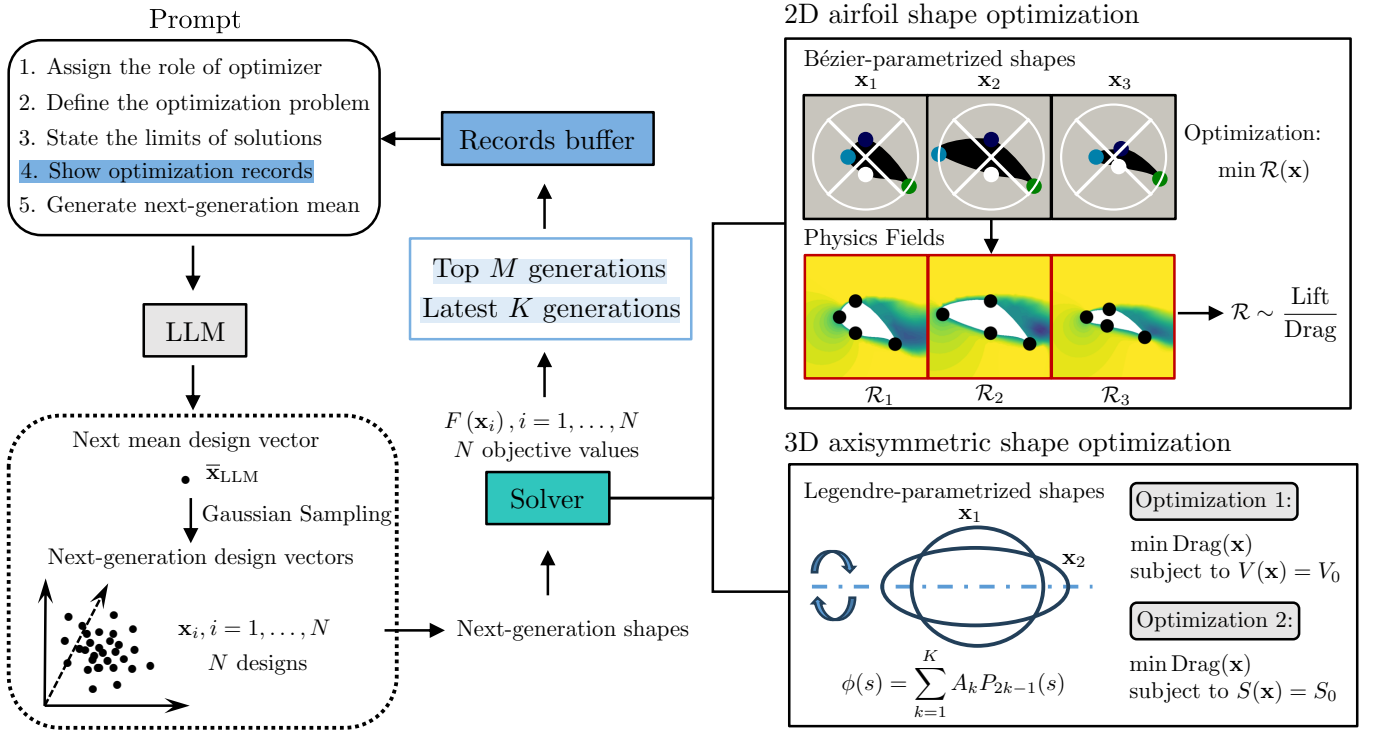


Fig. 1. Overview of LLM-PSO and its application to two PSO problems involving fluid dynamics.

III. METHODOLOGY

Inspired by [52] that employs LLMs for optimization in the spirit of evolutionary strategy, we introduce an LLM-based optimization framework named LLM-PSO. This framework is developed to address parametric shape optimization problems. For our implementation, we use the LLM “claude-3-5-sonnet-20240620” developed by Anthropic. Before delving into the details of LLM-PSO, we first define the optimization problem. A particular design is geometrically parametrized by a vector \mathbf{x} , which encodes all optimizable design variables. Using LLM-PSO, we seek the optimal design

$$\mathbf{x}^* = \underset{\mathbf{x}}{\operatorname{argmax}} F(\mathbf{x}), \quad (1)$$

which maximizes the objective function $F(\mathbf{x})$ indicating the design performance.

A. Workflow of LLM-PSO

In the vein of evolutionary strategies [70], LLM-PSO functions by evolving a population of N designs $\{\mathbf{x}_i\}_{i=1}^N$ generation by generation. Its workflow is demonstrated in Fig. 1. For simplicity, we assume that the design vectors within one generation follows an N -dimensional Gaussian distribution with a mean $\bar{\mathbf{x}}$ and fixed variance matrix $\sigma^2 \mathbf{I}$, *i.e.*,

$$\mathbf{x} \sim \mathcal{N}(\bar{\mathbf{x}}, \sigma^2 \mathbf{I}). \quad (2)$$

We start the optimization by initializing the first n_{ini} generations of design vectors. These generations are sampled from the afore-mentioned Gaussian distribution, with its mean $\bar{\mathbf{x}}$ seeded randomly within a range specific to case. Then we evaluate the objective function $F(\mathbf{x})$, *i.e.*, the performance for each initial design \mathbf{x} , and store the design-performance pair, $[\mathbf{x}, F(\mathbf{x})]$, of all such designs in a record buffer.

Subsequently, LLM guides the searching of the optimal design. First, we prepare a prompt (see Sec. III A 1) that encompasses selected design-performance records from the buffer; the selection strategy is detailed in Sec. III A 2. The prompt demonstrates these selections to the LLM, which returns a mean $\bar{\mathbf{x}}_{\text{LLM}}$ for the next generation. Then, resampling from the Gaussian distribution with this mean $\bar{\mathbf{x}}_{\text{LLM}}$ yields a new generation of designs. Next, we assess these designs’ performance and append the paired design-performance data to the record buffer. The augmented buffer contributes to the prompt preparation for the following generation, thus beginning a new iteration.

1. Overview of the prompt

We develop for LLM-PSO a few-shot prompting architecture consisting of five parts:

1. Assign the task of evolutionary optimization to the LLM;

2. Specify the dimensions of the design vector and the optimization objective;
3. Delineate the parameter range for optimization;
4. Supply the LLM with selected records and direct it to suggest the most promising mean $\bar{\mathbf{x}}_{\text{LLM}}$ for the subsequent generation;
5. Instruct the LLM to present this mean $\bar{\mathbf{x}}_{\text{LLM}}$ in a specified format.

An example prompt is shown in Fig. 2.

2. Strategy of records selection

Design-performance records are selectively included in the fourth part of the prompt, expressed in natural language. The selection process is as follows. Firstly, we sort the designs within each generation in ascending order based on their objective functions $F(\mathbf{x})$. Next, we rank the generations in ascending order according to the best design (*i.e.*, the one with the highest $F(\mathbf{x})$) in each generation. We then identify the top-ranking T generations and the most recent R generations, removing overlaps. For each of these identified generations, only the top-ranking M designs are selected to be included in the prompt.

B. Other details

Due to the limitations of LLMs in handling floating-point numbers effectively, we transform the values within the design vectors into integers [38, 52] ranged from 0 to 1000 before querying the LLM. To further ensure the stability of the outputs, we set the temperature parameter to 0, thereby forcing the LLM to generate deterministic results by consistently selecting the highest-probability output.

IV. RESULTS AND OBSERVATIONS

We employ LLM-PSO to tackle two representative optimization tasks in fluid dynamics and benchmark our results against those obtained using other algorithms. Specifically, we seek the optimal shapes of a two-dimensional (2D) airfoil and a three-dimensional (3D) axisymmetric body in fluid flow.

A. Two-dimensional airfoil shape optimization

We apply our strategy to a classical setting—optimizing the shape of a 2D airfoil to maximize its aerodynamic performance at a moderate Reynolds (Re)

Prompt Example

Role: You are an evolutionary optimizer.
 Task: You will MAXIMIZE a function $F[x, y, e]$ with 3 variables x, y, e .
 Range: x, y, e range between $[0, 1000]$.
 Records: Below are the records of the top-performing generations of $[x, y, e]$ values. Each line of records represents one generation. Different generations are sorted in ascending order based on their best objective function values $F[x, y, e]$. Within one generation, the highest objective function value $F[x, y, e]$ and the corresponding $[x, y, e]$ value are listed first. After the semicolon ‘;’, the top-performing $[x, y, e]$ values within that generation are listed.
 -0.055657:[281,244,711]; [265,315,772]...[281,244,711]
 -0.022432:[764,664,841]; [874,668,707]...[764,664,841]
 0.039566:[376,622,563]; [348,506,986]...[376,622,563]
 0.068052:[428,768,902]; [293,699,880]...[428,768,902]
 0.226759:[673,187,908]; [664,277,878]...[673,187,908]
 0.481255:[965,239,982]; [909,430,934]...[965,239,982]
 Determine a new $[x, y, e]$ value for the next generation to achieve higher $F[x, y, e]$ values. Format your output in $[x, y, e]$. No explanation needed.

Fig. 2. A specific example prompt of LLM-PSO.

number. This problem [32] was previously addressed using RL. In our study, we adopt the same setting but replace the RL-based optimizer with our LLM-based version, LLM-PSO.

1. Shape parametrization

We parameterize the airfoil profile by a Bézier curve connecting four control points indexed $i \in \{0, 1, 2, 3\}$. The i -th point is characterized by its Cartesian coordinates (x_i, y_i) and a sharpness factor e_i (see SI) of the Bézier curve at this point. Here, the coordinates have been non-dimensionalized by a characteristic length ℓ ; the same applies to other coordinates or length scales from hereinafter.

We then introduce a polar coordinate system (ρ, θ) equally partitioned into four sectors in analogous to a pie chart, see Fig. 3(a). Each control point, for example the i -th with coordinates (ρ_i, θ_i) , is restricted exclusively to one distinct sector, namely, $\theta_i \in [-\frac{\pi}{8} + \frac{\pi}{4}i, \frac{\pi}{8} + \frac{\pi}{4}i]$. This restriction is imposed to reduce the occurrence of entangled airfoil profiles. Here, $\rho_i = \sqrt{x_i^2 + y_i^2}$ and $(x_i, y_i) = \rho_i (\cos \theta_i, \sin \theta_i)$. Further, (ρ_i, θ_i, e_i) is transformed to a three-element vector $(p_i, q_i, m_i) \in [-1, 1]^3$,

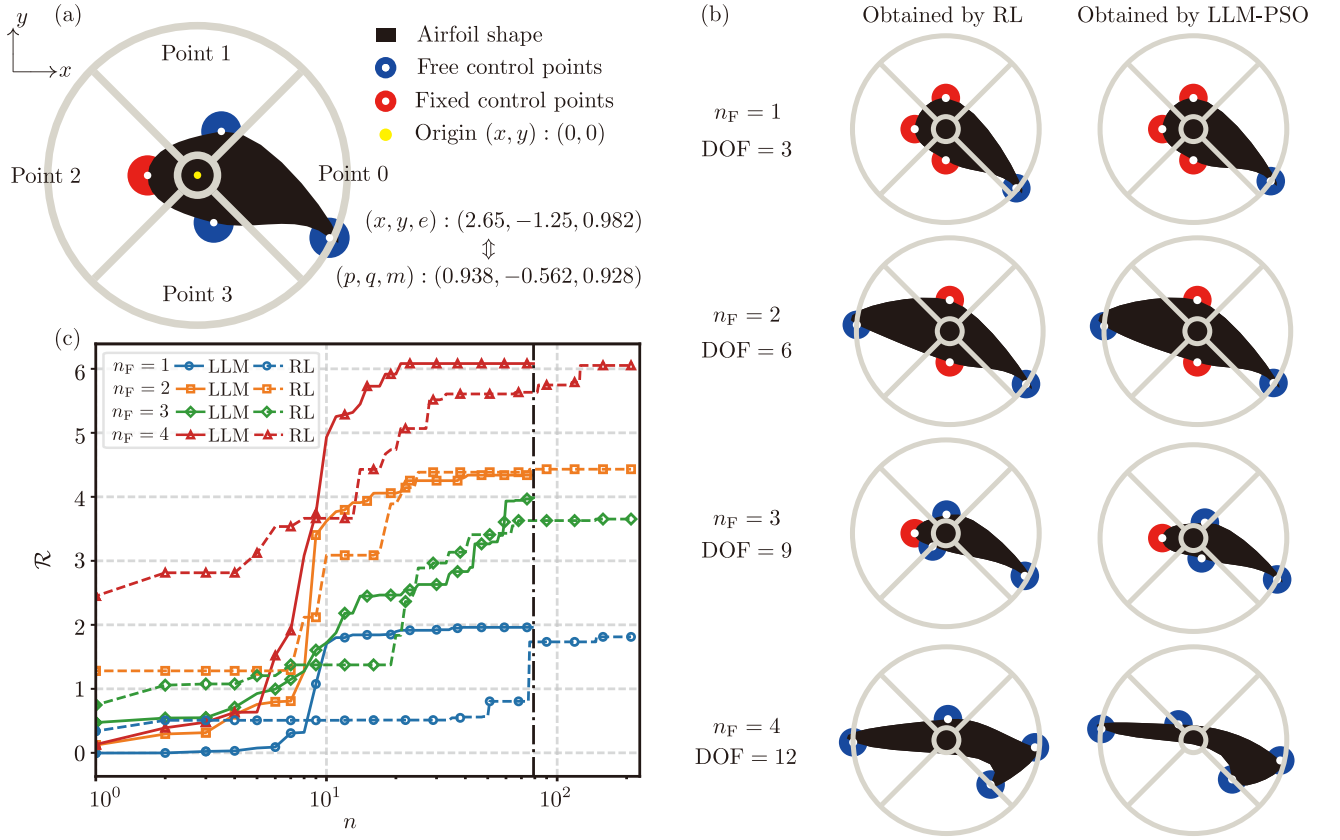


Fig. 3. (a) Geometric parametrization of an airfoil profile by a four-point Bézier curve. (b) Optimal airfoils based on different number $n_F \in [1, 4]$ of free points. (c) Comparison of the optimization trajectories: the lift-drag ratio versus iteration number $\mathcal{R}(n)$, between LLM-PSO and an RL algorithm [32].

$$p_i = 2 \left(\frac{\rho_i - \rho_{\min}}{\rho_{\max} - \rho_{\min}} \right) - 1, \quad (3a)$$

$$q_i = 2 \left(\frac{4}{\pi} \theta_i - i \right), \quad (3b)$$

$$m_i = 2e_i - 1, \quad (3c)$$

where $\rho_{\min} = 0.6$ and $\rho_{\max} = 3$ set the size of airfoils.

2. Optimization setup

Using an open-source finite-element-method solver, FEniCS [71] for partial differential equations, we solve the dimensionless Navier-Stokes equation to evaluate an airfoil's aerodynamic performance (see SI). Specifically, we focus on the ratio, f_L/f_D , of its aerodynamic lift f_L to drag f_D . In this study, we fix the Reynolds number to $Re = 100$, with 2ℓ serving as the characteristic length scale. At this Reynolds number, the flow past an airfoil is typically unsteady and periodic. To faithfully evaluate the performance, a simulation is first run to reach a time-periodic state. We then extract the time-averaged lift-to-drag ratio $\langle f_L/f_D \rangle$ as the performance indicator.

Choosing a cylinder of radius ℓ as the baseline design, our optimization aims to maximize the relative lift-to-drag ratio, namely,

$$\bar{\mathcal{R}} = \left\langle \frac{f_L}{|f_D|} \right\rangle - \left\langle \frac{f_L}{|f_D|} \right\rangle_{\text{cyl}}. \quad (4)$$

For benchmark purposes, we adhere to [32] in choosing the objective function for optimization:

$$\mathcal{R} = \begin{cases} 2\bar{\mathcal{R}}, & \bar{\mathcal{R}} > 0, \\ \bar{\mathcal{R}}, & \bar{\mathcal{R}} < 0, \\ -5, & \text{when simulation fails.} \end{cases} \quad (5)$$

Accordingly, we will seek the optimal shape parametrization $\mathbf{x}^* = \underset{\mathbf{x}}{\operatorname{argmax}} \mathcal{R}(\mathbf{x})$ leading to the maximum ratio.

3. Optimal airfoil profiles

In the optimization, we fix certain control points and free the remaining n_F points for optimization. Because each free point has three degrees of freedom (DOFs), the total number of optimization DOFs varies from three to

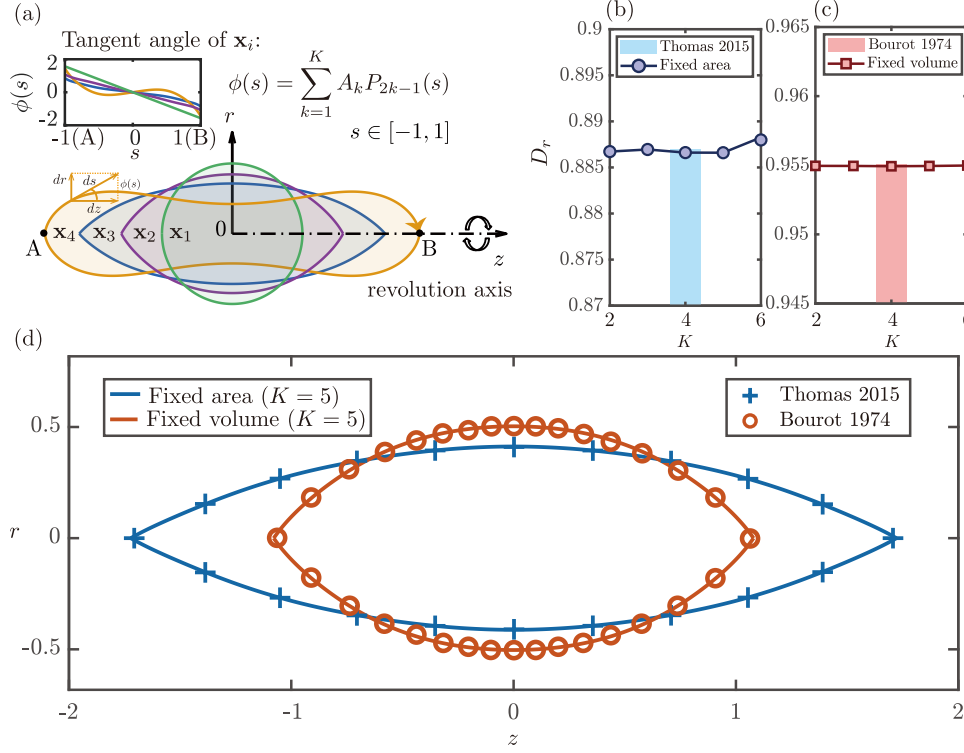


Fig. 4. (a) Parametrization of the 2D profile of an axisymmetric body using Legendre polynomials. The normalized drag D_r averaged over five LLM-PSO-based optimizations versus the number K of DOFs, when the (b) surface area or (c) volume of the body is fixed. The results are compared to theoretical solutions. (d) LLM-obtained optimal profiles (solid curve) in comparison to theoretical counterparts (symbol).

twelve, corresponding to $n_F = 1$ to $n_F = 4$ optimizable control points, respectively. An example of $n_F = 3$ is shown in Fig. 3(a).

In this study, we vary n_F within the set $\{1, 2, 3, 4\}$ to conduct the optimization. The optimal shapes are illustrated in Fig. 3(b). Except for $n_F = 4$, which will be discussed separately below, the obtained optimal profiles resemble the shape of classical airfoils. Further, we compare in Fig. 3(c) the trajectories of the LLM-PSO-based and RL-based optimization approaches. To ensure a fair comparison of their convergence, the iteration number of the latter have been scaled by the population size of the former. Upon convergence, LLM achieves similar or slightly better optimization targets compared to RL for all cases. Notably, LLM converges faster than RL, by almost an order of magnitude when $n_F = 1$ and 4. We acknowledge that when $n_F = 4$, our LLM-PSO cannot reproduce the optimal shape reported in [32]. The observation suggests that, LLM-PSO may not perform effectively at a relatively large number of DOFs, a limitation we aim to address in future work. Nevertheless, it is worth-noting that the RL-based optimization does not achieve this shape either, a rarity confirmed through private communications with the authors of [32].

B. Drag minimization of a revolved body in Stokes flow

Now, we apply LLM-PSO to seek the optimal profile of a 3D axisymmetric body for minimizing its hydrodynamic drag in Stokes flow. This optimization problem has been addressed theoretically by fixing the volume V [72] or surface area S [73] of the body. The resulting optimal profiles can be used to validate our optimal solutions. Besides, we will use the classical genetic algorithm (GA) to conduct the optimization, considering that LLM-PSO is inspired by the principles of evolutionary algorithms.

To be general, we describe the optimization problem in the dimensionless form, choosing $\ell = \left(\frac{3V_0}{4\pi}\right)^{1/3}$ as the characteristic length scale for the case when the prescribed volume is V_0 . In the alternative scenario where the surface area is fixed at S_0 , we adopt $\ell = \left(\frac{S_0}{4\pi}\right)^{1/2}$. In both cases, ℓ represents the radius of a sphere with the specified volume V_0 or area S_0 .

1. Shape parametrization

As shown in Fig. 4(a), the axisymmetric 3D body Ω is characterized by a 2D profile in the rz -plane. The z -

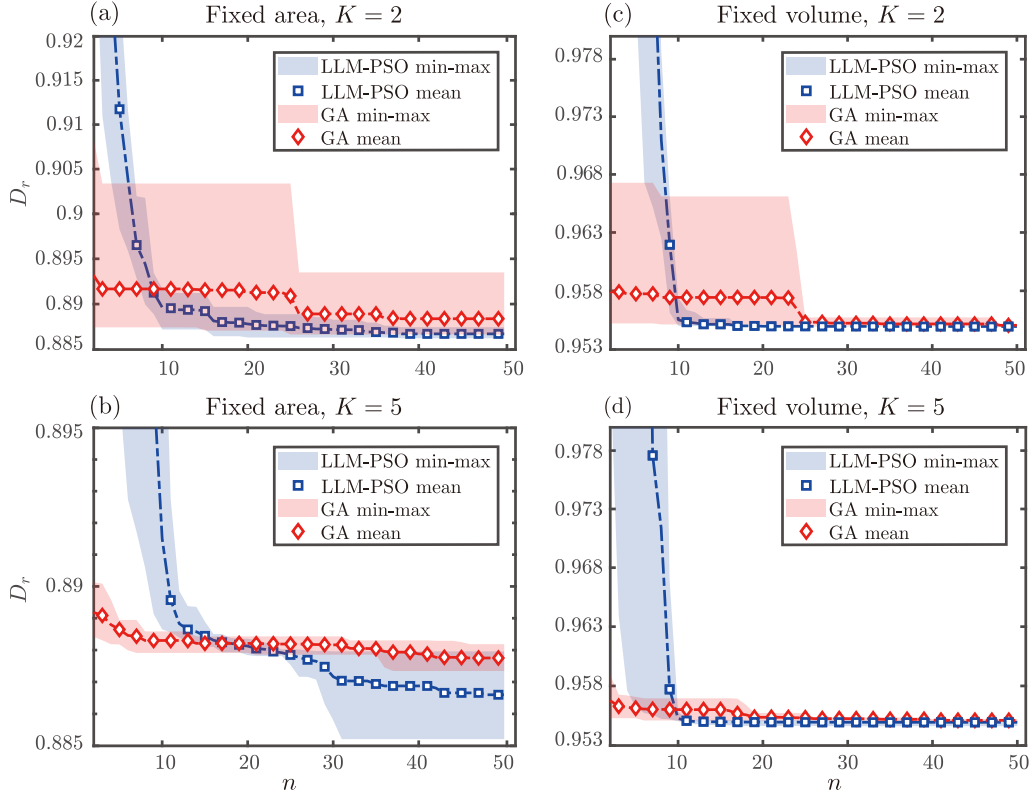


Fig. 5. Comparison of the performance of LLM-PSO and GA based on their optimization trajectories: the normalized drag versus iteration number $D_r(n)$, represented by mean values and min-max ranges from five runs. The left and right columns present results for area-fixed and volume-fixed settings, respectively, while the top and bottom rows correspond to $K = 2$ and $K = 5$ degrees of freedom, respectively. To ensure a fair comparison, we adopt the same population size N for LLM-PSO and GA.

axis coincides with the revolution axis, and r represents the radial coordinate. This profile can be characterized by its tangent angle $\phi(s)$ as a function of the arclength $s \in [-1, 1]$. Employing Legendre expansion as in [73], the angle is parameterized by

$$\phi(s) = \sum_{k=1}^K A_k P_{2k-1}(s), \quad (6)$$

which involves a number of K odd Legendre polynomials P_{2k-1} with corresponding coefficients A_k . The coefficients A_1, A_2, \dots, A_K together constitute the K -dimensional design vector \mathbf{x} for this optimization case,

$$\mathbf{x} = [A_1 \ A_2 \ \dots \ A_K]. \quad (7)$$

With $\phi(s)$ determined by \mathbf{x} , the 2D profile $(r(s), z(s))$ can then be obtained:

$$r(s) = \lambda \int_{-1}^s \sin \phi(\tilde{s}) d\tilde{s}, \quad z(s) = \lambda \int_{-1}^s \cos \phi(\tilde{s}) d\tilde{s}. \quad (8)$$

Notably, a scaling factor λ is needed to ensure that the obtained body of revolution satisfies the prescribed volume or area constraints.

2. Optimization setup

We perform two types of shape optimization to minimize the drag D over the body, either with a constraint on its volume V [72] or surface area S [73]. To calculate the drag D , we numerically solve the axisymmetric Stokes equation using the PDE mode of COMSOL Multiphysics 5.5 (I-Math, Singapore). We discretize a square computational domain sized 1000ℓ by approximately 26000 triangular Taylor-Hood elements, with local refinement near the body surface. We impose no-slip boundary condition at the body surface, a uniform velocity at the inlet, and a zero-pressure at the outlet.

3. Optimal profiles

Using the algorithm and fixing either the area or the volume of the body of revolution, we determine its drag-minimizing profiles for mode numbers $K \in [2, 6]$. Their drags, normalized by the reference drag of a sphere with the same area or volume, are denoted as D_r , as presented in Fig. 4(b) for the area-fixed case and Fig. 4(c) for the volume-fixed case, respectively. As indicated, the mini-

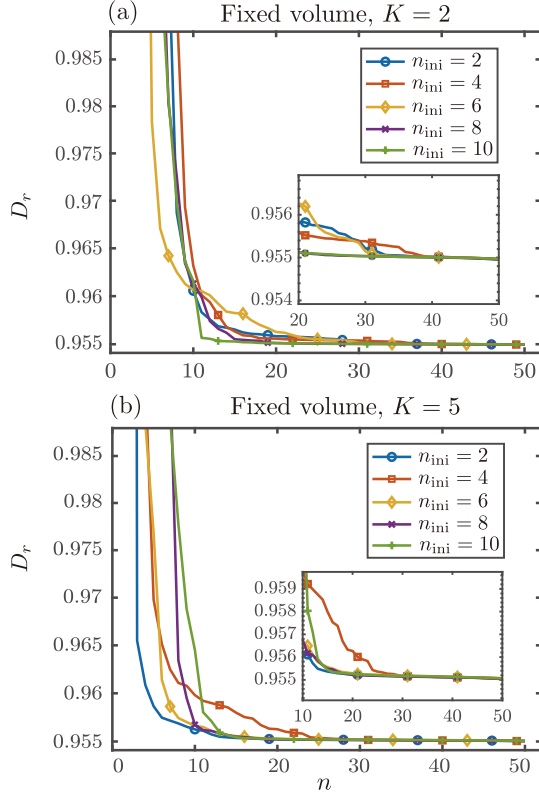


Fig. 6. The influence of the number n_{ini} of randomly seeded initial generations on the optimization trajectory $D_r(n)$ for (a) $K = 2$ and (b) $K = 5$. For each case, five runs are conducted to obtain a mean trajectory.

mal drags we obtain closely match with the theoretical optimal solutions [72, 73]. Naturally, the corresponding 2D profiles from our optimization, such as those at $K = 5$, show excellent agreement with the benchmark profiles. These consistent results demonstrate the effectiveness of our optimization strategy.

We further compare the performance of LLM-PSO to that of GA in Fig. 5 for $K = 2$ (upper panels) and $K = -5$ (lower panels). For comparison, we use the same population size N for both algorithms and conduct five runs for each optimization task. In the optimization's very early stage *i.e.*, $n \lesssim 5$, LLM-PSO performs worse than GA—the drag D_r is higher in the former case. However, by $n \approx 10$, LLM-PSO surpasses GA, exhibiting a steep decline in D_r . Consequently, LLM-PSO achieves a slightly better target value, *viz.*, a lower mean drag D_r averaged over the five runs. In addition, LLM-PSO exhibits a smaller statistical variance than GA when $K = 2$. However, this trend reverses when K increases to 5.

Finally, in Fig. 6, we examine the influence of n_{ini} on the optimization process for the volume-fixed setting. The converged minimal drag D_r is shown to be independent of n_{ini} . When $K = 2$, the optimization trajectories are weakly affected by n_{ini} , without revealing a clear trend. As K increases to 5, we observe that a lower n_{ini}

leads to faster initial convergence.

V. CONCLUSIONS AND DISCUSSIONS

We have developed a novel LLM-based framework LLM-PSO that marries generative AI with evolutionary strategy for parametric shape optimization. This framework leverages the emerging ICL capacity of LLMs to assist decision-making. To demonstrate its effectiveness, we employed LLM-PSO to identify drag-minimizing profiles of a 2D airfoil in laminar flow and a 3D axisymmetric body in Stokes flow. In both cases, LLM-PSO successfully determined optimal shapes that align with established benchmark profiles.

We acknowledge that certain hyperparameters of LLM-PSO have not been thoroughly investigated. For instance, the number of top-ranking designs M displayed in each generation warrants additional test. Further fine-tuning these hyperparameters may enhance the optimization performance of LLM-PSO.

Based on the current success of LLM-PSO, we point several potential research directions: 1) Improving the current LLM-PSO to address shape optimization with high DOFs; 2) Employing fine-tuning techniques to enhance the optimization capabilities of LLMs; 3) Combining other advanced optimization algorithm with LLMs to achieve synergistic enhancement in performance.

SUPPLEMENTARY INFORMATION

Sharpness factor in Bézier parametrization

The sharpness factor plays a key role in controlling the tangent angle of the generated Bézier curve at a specific control point. Take the i -th point for example: We first define the relative angular orientations of point i with respect to its two neighboring points as $\theta_{i,i-1} = \arctan\left(\frac{y_i - y_{i-1}}{x_i - x_{i-1}}\right)$ for point i relative to point $i - 1$ and $\theta_{i,i+1} = \arctan\left(\frac{y_{i+1} - y_i}{x_{i+1} - x_i}\right)$ for point i relative to point $i + 1$; Then, using these relative angles, the sharpness factor e_i determines the tangent angle θ_i^* at point i , which is a weighted combination of the two neighboring angles:

$$\theta_i^* = e_i \theta_{i-1,i} + (1 - e_i) \theta_{i,i+1}. \quad (\text{A.1})$$

Simulation for flow past a 2D airfoil

To calculate the lift-to-drag ratio of a certain airfoil design [32], we numerically solve the Navier-Stokes equations using the open-source PDE solver FEniCs [71]. We adopt an rectangular computational domain of size $45\ell \times 30\ell$, where ℓ represents the radius of the cylinder as the baseline design. A no-slip boundary condition is applied at the airfoil surface, a uniform velocity condition at the inlet, and a zero-pressure condition at the outlet. We utilize Gmsh [74] to generate the mesh for this simulation.

Data Availability

The datasets used and/or analyzed during the current study available from the corresponding author on reasonable request.

Code Availability

The prompt along with the related source codes will be open-sourced upon the acceptance of this manuscript.

- [1] J. Li, M. Zhang, J. R. Martins, and C. Shu, "Efficient aerodynamic shape optimization with deep-learning-based geometric filtering," *AIAA J.*, vol. 58, no. 10, pp. 4243–4259, 2020.
- [2] H. Zong, H. Zhang, Y. Wang, M. Y. Wang, and J. Y. Fuh, "On two-step design of microstructure with desired Poisson's ratio for AM," *Mater. Des.*, vol. 159, pp. 90–102, 2018.
- [3] J. Gong, L. W. Chew, and P. S. Lee, "Shape optimization of high-rise solar chimneys to improve the uniformity of flowrate distribution," *Build. Environ.*, vol. 243, p. 110650, 2023.
- [4] B. B. Kanbur, S. Suping, and F. Duan, "Design and optimization of conformal cooling channels for injection molding: a review," *J. Adv. Manuf. Technol.*, vol. 106, no. 7, pp. 3253–3271, 2020.
- [5] J. Chen, G. Adit, L. Li, Y. Zhang, D. H. Chua, and P. S. Lee, "Optimization strategies toward functional sodium-ion batteries," *Energy Environ. Mater.*, vol. 6, no. 4, p. e12633, 2023.
- [6] A. Ammar, A. Huerta, F. Chinesta, E. Cueto, and A. Leygue, "Parametric solutions involving geometry: a step towards efficient shape optimization," *Comput. Methods Appl. Mech. Eng.*, vol. 268, pp. 178–193, 2014.
- [7] S. D. Daxini and J. M. Prajapati, "Parametric shape optimization techniques based on meshless methods: A review," *Struct. Multidiscip. Optim.*, vol. 56, pp. 1197–1214, 2017.
- [8] L.-W. Chen, B. A. Cakal, X. Hu, and N. Thuerey, "Numerical investigation of minimum drag profiles in laminar flow using deep learning surrogates," *J. Fluid Mech.*, vol. 919, p. A34, 2021.
- [9] P. Pedersen and C. L. Laursen, "Design for minimum stress concentration by finite elements and linear programming," *J. Struct. Mech.*, vol. 10, no. 4, pp. 375–391, 1982.
- [10] S. Jakobsson and O. Amoignon, "Mesh deformation using radial basis functions for gradient-based aerodynamic shape optimization," *Comput. Fluids.*, vol. 36, no. 6, pp. 1119–1136, 2007.
- [11] E. Ramm, K.-U. Bletzinger, and R. Reiteringer, "Shape optimization of shell structures," *Revue Européenne des Éléments Finis*, vol. 2, no. 3, pp. 377–398, 1993.
- [12] K.-D. Lee and K.-Y. Kim, "Shape optimization of a fan-shaped hole to enhance film-cooling effectiveness," *Int. J. Heat Mass Transf.*, vol. 53, no. 15–16, pp. 2996–3005, 2010.
- [13] X. Tang, W. Yang, Z. Dai, and Y. Yang, "Inverse design of local solar flux distribution for a solar methanol reforming reactor based on shape optimization," *Front. Energy Res.*, vol. 10, p. 881822, 2022.
- [14] D. J. Munk, G. A. Vio, and G. P. Steven, "Topology and shape optimization methods using evolutionary algorithms: a review," *Struct. Multidiscip. Optim.*, vol. 52, pp. 613–631, 2015.
- [15] S. Y. Woon, O. M. Querin, and G. P. Steven, "Structural application of a shape optimization method based on a genetic algorithm," *Struct. Multidiscip. Optim.*, vol. 22, pp. 57–64, 2001.
- [16] Y.-C. Chang, L.-J. Yeh, M.-C. Chiu, and G.-J. Lai, "Shape optimization on constrained single-layer sound absorber by using GA method and mathematical gradient methods," *J. Sound Vib.*, vol. 286, no. 4–5, pp. 941–961, 2005.
- [17] J. Hsiao, K. Shivam, C. Chou, and T. Kam, "Shape design optimization of a robot arm using a surrogate-based evolutionary approach," *Appl. Sci.*, vol. 10, no. 7, p. 2223, 2020.
- [18] F. O. Sonmez, "Shape optimization of 2D structures using simulated annealing," *Comput. Methods Appl. Mech. Eng.*, vol. 196, no. 35–36, pp. 3279–3299, 2007.
- [19] G. S. Kumar, A. Mahendra, and G. Gouthaman, "Multi-objective shape optimization using ant colony coupled computational fluid dynamics solver," *Comput. Fluids.*, vol. 46, no. 1, pp. 298–305, 2011.
- [20] X.-S. Yang and A. Hossein Gandomi, "Bat algorithm: a novel approach for global eng. optim." *Eng. Comput.*, vol. 29, no. 5, pp. 464–483, 2012.
- [21] S. Gholizadeh and A. Barzegar, "Shape optimization of structures for frequency constraints by sequential harmony search algorithm," *Eng. Optim.*, vol. 45, no. 6, pp. 627–646, 2013.
- [22] A. Khalilnejad, A. Sundararajan, and A. I. Sarwat, "Optimal design of hybrid wind/photovoltaic electrolyzer for maximum hydrogen production using imperialist competitive algorithm," *J. Mod. Power Syst. Clean Energy.*, vol. 6, no. 1, pp. 40–49, 2018.
- [23] J. Li, X. Du, and J. R. Martins, "Machine learning in aerodynamic shape optimization," *Prog. Aerosp. Sci.*, vol. 134, p. 100849, 2022.
- [24] F. Ding and A. Kareem, "A multi-fidelity shape optimization via surrogate modeling for civil structures," *J. Wind Eng. Ind. Aerodyn.*, vol. 178, pp. 49–56, 2018.
- [25] K. Ezhilsabareesh, S. H. Rhee, and A. Samad, "Shape optimization of a bidirectional impulse turbine via surrogate models," *Eng. Appl. Comput. Fluid Mech.*, vol. 12, no. 1, pp. 1–12, 2018.
- [26] P. LeGresley and J. Alonso, "Airfoil design optimization using reduced order models based on proper orthogonal decomposition," in *Fluids 2000 Conference and Exhibit*, 2000, p. 2545.
- [27] M. Xiao, P. Breittkopf, R. Filomeno Coelho, C. Knopf-Lenoir, M. Sidorkiewicz, and P. Villon, "Model reduction by CPOD and Kriging: application to the shape optimization of an intake port," *Struct. Multidiscip. Optim.*, vol. 41, pp. 555–574, 2010.
- [28] S. Ghoman, Z. Wang, P. Chen, and R. Kapania, "A POD-based reduced order design scheme for shape optimization of air vehicles," in *53rd AIAA/ASME/ASCE/AHS/ASC Structures, Structural Dynamics and Materials Conference 20th AIAA/ASME/AHS Adaptive Structures Conference 14th AIAA*, 2012, p. 1808.
- [29] J. Kober, J. A. Bagnell, and J. Peters, "Reinforcement learning in robotics: A survey," *Int. J. Robot. Res.*, vol. 32, no. 11, pp. 1238–1274, 2013.
- [30] D. Silver, J. Schrittwieser, K. Simonyan, I. Antonoglou, A. Huang, A. Guez, T. Hubert, L. Baker, M. Lai, A. Bolton *et al.*, "Mastering the game of Go without human knowledge," *Nature*, vol. 550, no. 7676, pp. 354–359, 2017.

- [31] X. Yan, J. Zhu, M. Kuang, and X. Wang, "Aerodynamic shape optimization using a novel optimizer based on machine learning techniques," *Aerosp. Sci. Technol.*, vol. 86, pp. 826–835, 2019.
- [32] J. Viquerat, J. Rabault, A. Kuhnle, H. Ghraieb, A. Larcher, and E. Hachem, "Direct shape optimization through deep reinforcement learning," *J. Comput. Phys.*, vol. 428, p. 110080, 2021.
- [33] T. P. Dussauge, W. J. Sung, O. J. Pinon Fischer, and D. N. Mavris, "A reinforcement learning approach to airfoil shape optimization," *Sci. Rep.*, vol. 13, no. 1, p. 9753, 2023.
- [34] H. Keramati, F. Hamdullahpur, and M. Barzegari, "Deep reinforcement learning for heat exchanger shape optimization," *Int. J. Heat Mass Transf.*, vol. 194, p. 123112, 2022.
- [35] J. Wei, Y. Tay, R. Bommasani, C. Raffel, B. Zoph, S. Borgeaud, D. Yogatama, M. Bosma, D. Zhou, D. Metzler *et al.*, "Emergent abilities of large language models," *arXiv preprint arXiv:2206.07682*, 2022.
- [36] Q. Dong, L. Li, D. Dai, C. Zheng, J. Ma, R. Li, H. Xia, J. Xu, Z. Wu, T. Liu *et al.*, "A survey on in-context learning," *arXiv preprint arXiv:2301.00234*, 2022.
- [37] Y.-J. Wang, B. Zhang, J. Chen, and K. Sreenath, "Prompt a robot to walk with large language models," *arXiv preprint arXiv:2309.09969*, 2023.
- [38] Z. Xu and L. Zhu, "Training microrobots to swim by a large language model," *arXiv preprint arXiv:2402.00044*, 2024.
- [39] L. Song, C. Zhang, L. Zhao, and J. Bian, "Pre-trained large language models for industrial control," *arXiv preprint arXiv:2308.03028*, 2023.
- [40] P.-F. Guo, Y.-H. Chen, Y.-D. Tsai, and S.-D. Lin, "Towards optimizing with large language models," *arXiv preprint arXiv:2310.05204*, 2023.
- [41] C. Yang, X. Wang, Y. Lu, H. Liu, Q. V. Le, D. Zhou, and X. Chen, "Large language models as optimizers," 2024. [Online]. Available: <https://arxiv.org/abs/2309.03409>
- [42] M. R. Zhang, N. Desai, J. Bae, J. Lorraine, and J. Ba, "Using large language models for hyperparameter optimization," in *NeurIPS 2023 Foundation Models for Decision Making Workshop*, 2023.
- [43] M. J. Buehler, "MechGPT, a language-based strategy for mechanics and materials modeling that connects knowledge across scales, disciplines, and modalities," *Appl. Mech. Rev.*, vol. 76, no. 2, p. 021001, 2024.
- [44] V. Kumar, L. Gleyzer, A. Kahana, K. Shukla, and G. E. Karniadakis, "MyCrunchGPT: A ChatGPT assisted framework for scientific machine learning," *arXiv preprint arXiv:2306.15551*, 2023.
- [45] D. Kim, T. Kim, Y. Kim, Y.-H. Byun, and T. S. Yun, "A ChatGPT-MATLAB framework for numerical modeling in geotechnical engineering applications," *Comput. Geotech.*, vol. 169, p. 106237, 2024.
- [46] Y. Chena, X. Zhua, H. Zhoua, and Z. Rena, "MetaOpenFOAM: an LLM-based multi-agent framework for CFD," *arXiv preprint arXiv:2407.21320*, 2024.
- [47] M. Du, Y. Chen, Z. Wang, L. Nie, and D. Zhang, "Large language models for automatic equation discovery of nonlinear dynamics," *Phys. Fluids*, vol. 36, no. 9, 2024.
- [48] M. Zhu, A. Bazaga, and P. Liò, "FLUID-LLM: Learning computational fluid dynamics with spatiotemporal-aware large language models," *arXiv preprint arXiv:2406.04501*, 2024.
- [49] B. Li, K. Mellou, B. Zhang, J. Pathuri, and I. Menache, "Large language models for supply chain optimization," *arXiv preprint arXiv:2307.03875*, 2023.
- [50] S. Liu, C. Chen, X. Qu, K. Tang, and Y.-S. Ong, "Large language models as evolutionary optimizers," in *2024 IEEE Congress on Evolutionary Computation (CEC)*. IEEE, 2024, pp. 1–8.
- [51] S. Brahmachary, S. M. Joshi, A. Panda, K. Koneripalli, A. K. Sagotra, H. Patel, A. Sharma, A. D. Jagtap, and K. Kalyanaraman, "Large language model-based evolutionary optimizer: Reasoning with elitism," *arXiv preprint arXiv:2403.02054*, 2024.
- [52] R. Lange, Y. Tian, and Y. Tang, "Large language models as evolution strategies," in *Proceedings of the Genetic and Evolutionary Computation Conference Companion*, 2024, pp. 579–582.
- [53] T. Liu, N. Astorga, N. Seedat, and M. van der Schaar, "Large language models to enhance Bayesian optimization," *arXiv preprint arXiv:2402.03921*, 2024.
- [54] H. Ye, J. Wang, Z. Cao, and G. Song, "Reevo: Large language models as hyper-heuristics with reflective evolution," *arXiv preprint arXiv:2402.01145*, 2024.
- [55] X. Wu, S.-h. Wu, J. Wu, L. Feng, and K. C. Tan, "Evolutionary computation in the era of large language model: Survey and roadmap," *arXiv preprint arXiv:2401.10034*, 2024.
- [56] R. Zhong, Y. Xu, C. Zhang, and J. Yu, "Leveraging large language model to generate a novel metaheuristic algorithm with CRISPE framework," *Cluster Comput.*, pp. 1–35, 2024.
- [57] M. Pluhacek, A. Kazikova, T. Kadavy, A. Viktorin, and R. Senkerik, "Leveraging large language models for the generation of novel metaheuristic optimization algorithms," in *Proceedings of the Companion Conference on Genetic and Evolutionary Computation*, 2023, pp. 1812–1820.
- [58] F. Liu, X. Tong, M. Yuan, and Q. Zhang, "Algorithm evolution using large language model," *arXiv preprint arXiv:2311.15249*, 2023.
- [59] N. Yüksel, H. R. Börklü, H. K. Sezer, and O. E. Canyurt, "Review of artificial intelligence applications in engineering design perspective," *Eng. Appl. Artif. Intell.*, vol. 118, p. 105697, 2023.
- [60] W. Liao, X. Lu, Y. Fei, Y. Gu, and Y. Huang, "Generative AI design for building structures," *Autom. Constr.*, vol. 157, p. 105187, 2024.
- [61] Y. Wang, K. Shimada, and A. Barati Farimani, "Airfoil GAN: encoding and synthesizing airfoils for aerodynamic shape optimization," *J. Comput. Des. Eng.*, vol. 10, no. 4, pp. 1350–1362, 2023.
- [62] M. Usama, Z. Masood, S. Khan, K. Kostas, and P. Kaklis, "Generative vs non-generative models in engineering shape optimization," *arXiv preprint arXiv:2402.08540*, 2024.
- [63] F. Jiang, J. Ma, C. J. Webster, X. Li, and V. J. Gan, "Building layout generation using site-embedded GAN model," *Autom. Constr.*, vol. 151, p. 104888, 2023.
- [64] H. Jun and A. Nichol, "Shap-E: Generating conditional 3D implicit functions," *arXiv preprint arXiv:2305.02463*, 2023.
- [65] T. Rios, S. Menzel, and B. Sendhoff, "Large language and text-to-3D models for engineering design optimization," in *2023 IEEE Symposium Series on Computational Intelligence (SSCI)*. IEEE, 2023, pp. 1704–1711.

- [66] M. Wong, T. Rios, S. Menzel, and Y. S. Ong, “Prompt evolutionary design optimization with generative shape and vision-language models,” in *2024 IEEE Congress on Evolutionary Computation (CEC)*. IEEE, 2024, pp. 1–8.
- [67] G. Giannone, A. Srivastava, O. Winther, and F. Ahmed, “Aligning optimization trajectories with diffusion models for constrained design generation,” *Adv. Neural Inf. Process. Syst.*, vol. 36, pp. 51 830–51 861, 2023.
- [68] J. Chen, Z. Shao, and B. Hu, “Generating interior design from text: A new diffusion model-based method for efficient creative design,” *Buildings*, vol. 13, no. 7, p. 1861, 2023.
- [69] Z. Wei, E. R. Dufour, C. Pelletier, P. Fua, and M. Bauerheim, “DiffAirfoil: An efficient novel airfoil sampler based on latent space diffusion model for aerodynamic shape optimization,” in *AIAA AVIATION Forum and Ascend 2024*, 2024, p. 3755.
- [70] Z. Li, X. Lin, Q. Zhang, and H. Liu, “Evolution strategies for continuous optimization: A survey of the state-of-the-art,” *Swarm Evol. Comput.*, vol. 56, p. 100694, 2020.
- [71] M. Alnæs, J. Blechta, J. Hake, A. Johansson, B. Kehlet, A. Logg, C. Richardson, J. Ring, M. E. Rognes, and G. N. Wells, “The FEniCS project version 1.5,” *Archive of numerical software*, vol. 3, no. 100, 2015.
- [72] J.-M. Bourot, “On the numerical computation of the optimum profile in Stokes flow,” *J. Fluid Mech.*, vol. 65, no. 3, pp. 513–515, 1974.
- [73] T. D. Montenegro-Johnson and E. Lauga, “The other optimal Stokes drag profile,” *J. Fluid Mech.*, vol. 762, p. R3, 2015.
- [74] C. Geuzaine and J.-F. Remacle, “Gmsh: A 3D finite element mesh generator with built-in pre-and post-processing facilities,” *Int. J. Numer. Methods Eng.*, vol. 79, no. 11, pp. 1309–1331, 2009.